Crystallization

Deutsche Ausgabe: DOI: 10.1002/ange.201503052
Internationale Ausgabe: DOI: 10.1002/anie.201503052

In Situ Microscopic Observation of the Crystallization Process of Molecular Microparticles by Fluorescence Switching**

Xin Ye, Yang Liu, Yun Lv, Guangfeng Liu, Xiaoxin Zheng, Quanxiang Han, Kenneth A. Jackson, and Xutang Tao**

Abstract: *To clearly understand the solid-state amorphous-to-crystalline transformation is a long-standing challenge because such crystallization occuring in confined environments is difficult to observe directly. We developed an in situ and real-time imaging procedure to record the interface evolution in a solid-state crystallization of molecular amorphous particles. The method, by employing a tetra-substituted ethene with novel morphology-dependent fluorescence, which can distinguish the interfaces between the crystalline and amorphous phase by fluorescence color, is a simple and practical method to probe the inner process of a molecular microparticle. The crystallization of amorphous microparticles in different cases was clearly recorded, where the perfect microparticles and those with defects demonstrate diverse destinies. The details disclosed in this observation will deepen the understanding for a series of solid-state crystallization that we know little about before.*

The study of crystal formation is an ancient but essential subject, involving the study of the mechanisms of growth based on the observation of the interface of the crystal growing from its parent phase.[1] The mechanisms of crystal growth in materials such as metals and simple compounds are fairly well understood. Modeling and computer simulations have been used extensively for these materials. Since the growth process is relatively simple, large crystals can be grown in the laboratory.

Organic glasses are used in a number of diverse areas of technology, and so the amorphous-to-crystalline transformation [ACT] is important in a diversity of fields including semiconductor processing, geology, biomineralization, catalysis, and drug delivery.[2] It is thus important to understand the crystallization of these amorphous materials. Again, the process is fairly well understood in semiconductors, where for example thin film silicon solar cells are prepared by vapor depositing an amorphous layer of silicon and then crystalizing it. Direct deposit of silicon in crystalline form results in a very small crystal grain size and poor efficiency of the solar cell. However for complex molecular materials, such as drugs, the ACT process is much more complex than in semiconductors, and is not really understood.

The importance of understanding ACT for drug delivery has been emphasized by recent studies showing that for some drugs the therapeutic impact of the drug can be improved by delivering an amorphous form of the drug.[3] To utilize an amorphous drug delivery strategy, it is essential that the glassy form of the drug is maintained for the lifetime of the product, so the development of a fundamental understanding of crystallization tendency of these materials is needed. Baird et al.[4] contributed to this by evaluating the glass forming ability and glass stability of a large number of pharmaceutical molecules. Trasi et al.[5] studied crystal growth rates of many drugs from undercooled liquids. The crystallization rates were found to vary greatly for different kinds of compounds. This study demonstrated that there is still much yet to be learned about the crystallization of these materials. Such studies will enable discrimination of compounds that are at higher risk of crystallization from those that can be successful delivered in the glassy form.

The crystallization processes of large molecules are much more complex. Although the molecules in these materials are large, the crystals are usually very small and the growth process is difficult to observe directly in real systems. Crystal formation from solution or vapor phase can usually be directly observed.[6] however, for solid state crystallization, that is, for ACT, imaging of the growth process is difficult. The nucleation and growth in these transformations usually occurs in confined environments, and the interfaces of the newly formed crystals are buried in the solid body of the material, making the direct observation infeasible.[7]

Many advanced technologies have been employed to monitor the crystallization process in real time and under realistic growth conditions.[8] These significant studies of in situ imaging of crystal formation rely heavily on extremely high-tech instrumentation, nevertheless, they are still quite rare for ACT because of the ambiguous interface in the coexistence of amorphous/crystalline regions. An alternative approach has been to employ micro-colloidal particles in solutions or suspensions as model systems to study phase transitions and nucleation.[9] Although this method is simulated and not real, it has low requirements for experimental equipment since the process can be recorded using a normal optical microscope.

A novel method of resolving the crystalline/amorphous interface in an ACT would provide a facile way to distinguish

[*] X. Ye, Prof. Y. Liu, Y. Lv, G. Liu, X. Zheng, Q. Han, Prof. X. Tao
State Key Laboratory of Crystal Materials, Shandong University
Jinan, Shandong 250100 (P.R. China)
E-mail: liuyangicm@sdu.edu.cn
txt@sdu.edu.cn
K. A. Jackson
Department of Materials Science and Engineering
The University of Arizona, Tucson, AZ 85721 (USA)

[**] We thank the National Natural Science Foundation of China (Grant Nos. 51321091, 51227002, 51303095, 51272129) and the Program of Introducing Talents of Disciplines to Universities in China (111 program no. b06015).

Supporting information for this article is available on the WWW under http://dx.doi.org/10.1002/anie.201503052.

the two phases and subsequently to monitor the crystallization process. Enlightened by the probe of sub-cellular structures through cellular staining or the introduction of fluorescent proteins in biochemistry,[10] we tried to utilize a novel kind of compound discovered recently, and to design a procedure to do this. Some conjugate molecular materials have been found to exhibit distinct fluorescence colors in different solid states.[11] For example, as shown in Figure 1,

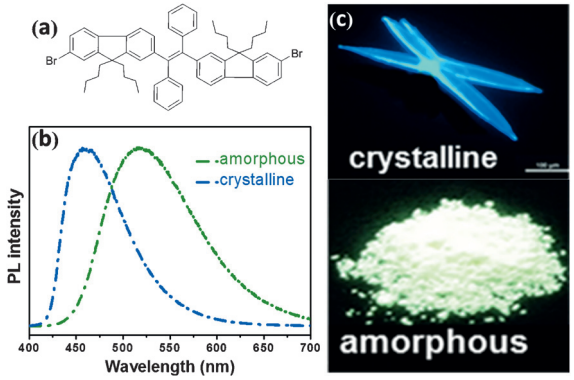

Figure 1. a) Chemical structure of 1,2-bis (7-bromo-9,9-dibutyl-fluorenyl)-1,2-diphenylethene (BBFT). b) Photoluminescence spectra and c) fluorescence images of BBFT, in different states (reproduced with permission from Ref. [13]).

a fluorenyl-containing tetrasubstituted ethylene: 1,2-bis(7-bromo-9,9-dibutyl-fluorenyl)-1,2-diphenylethene (BBFT), displays deep-blue color in crystals but greenish-yellow color in the amorphous state, with an emission difference of about 60 nm.[12] Further study indicates that the transformation between the two phases could proceed in mild conditions triggered by solvent vapor fuming.[13] In this study we use BBFT to develop a procedure to pry into the details of an ACT process by monitoring the fluorescence response of the material under a fluorescence microscope.

Figure 2 demonstrates the procedure of sample preparation and the observation procedure (for details, see the Supporting Information). The size of the microparticles could be tuned from hundreds of nanometer to approximately 10 micrometer by varying the solution concentration and the standing time[11i] (Supporting Information, Figure S1). To observe the microscopic aspects of the transformation process as far as possible, and taking account of the magnification of an optical microscope and the penetrability of the excitation and emission fluorescence, microspheres with dimensions of about 3 μm were finally employed in the observation experiments. Drop-casting the suspensions of BBFT onto a glass substrate followed by drying in the atmosphere results in an even distribution of the microspheres on the surface. As shown in Figure 3, the size of the aggregates formed is quite

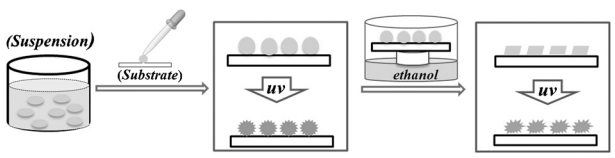

Figure 2. Sample preparation and the solvent fuming-induced amorphous-to-crystalline transformation accompanied by changing fluorescence response.

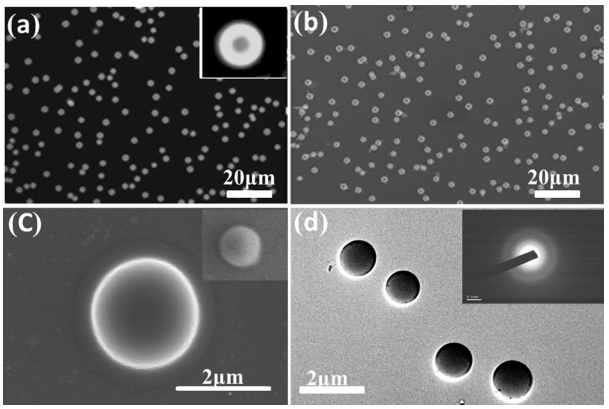

Figure 3. a) Images of BBFT microparticles on a glass substrate by fluorescence microscopy, b), c) SEM (inset: low detector), and d) TEM (inset: diffraction pattern).

uniform; and the spherical shape can be easily recognized in the amplified scanning electron microscopy (SEM) and transmission electron microscopy (TEM) images (Figure 3c,d). The intrinsic morphology of the microspheres was examined using selected-area electron diffraction on the TEM, where the microspheres showed no electron diffraction spots but only diffuse halos, manifesting their amorphous nature.

Another advantage of using BBFT to observe a solid-state phase transition through fluorescence response is its novel aggregation-induced emission (AIE) characteristic. The absolute fluorescence quantum yield of BBFT solid is greater than 90%, which is much higher than normal fluorescent dyes. Together with a high photostability, its merits greatly benefit fluorescent picture taking, especially for long time observation to avoid photo-beaching. The fluorescence microscope images of BBFT microparticles cast on a glass substrate are shown in Figure 3a. Besides their spherical shape, the green fluorescence was evidence of the amorphous nature of the microspheres.

To record the crystallization process in situ and real-time, a quartz vessel holding the samples and several milliliters of ethanol was placed on the object stage of the microscope (Figure 2). The ACT crystallization was induced by ethanol vapor fuming. We monitored the ACT process and recorded it with images based on both the appearance and the switching of the fluorescence of the microspheres during morphology development. The fluorescence images of the microspheres after certain periods of time were shown in Figure 4. Before exposure to ethanol vapor the microparticles display circular shapes and green fluorescence (Figure 4a). In the image, most of the individual microspheres display a relatively dark spot in the center, which is attributed to the direct contact of the particle surface with the substrate. After exposure to ethanol vapor for 10 h, the emission from the center part of the

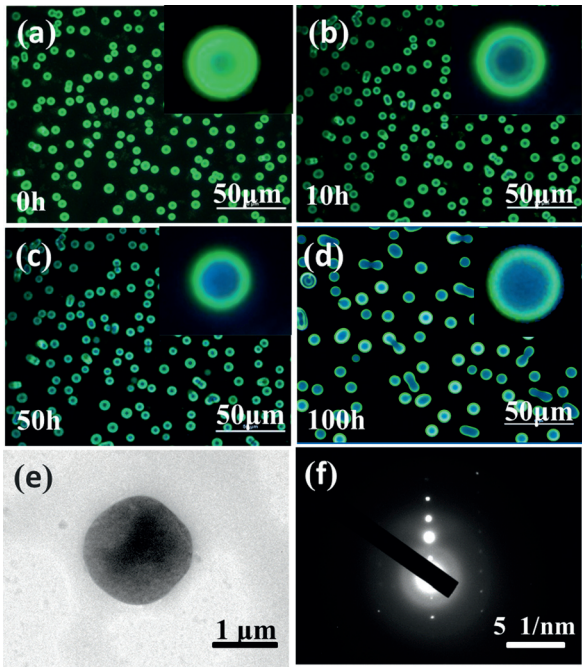

Figure 4. Fluorescence images of microparticles a) before and b)–d) after exposure to ethanol vapor for b) 10 h, c) 50 h, and d) 100 h. The four pictures were taken at the same location. inset: a single microparticle. e) TEM images of a microparticle after exposure to ethanol vapor for 50 h and f) the corresponding SAED pattern.

particle became blue (Figure 4b). Around the evident blue core, there is a ring with shallow blue fluorescence, which should be the intermediate state between the green amorphous and blue crystalline phase. As time goes on, the region with blue emissions becomes larger. After an exposure time of 50 h, the emission from most of the core part of each particle turned blue and the intermediate ring faded away (Figure 4c). The screenshot of the fluorescence image of a single microparticle in this stage is just like an annular eclipse, where the outer shell edges form a green ring around a blue ball. According to our previous work discussed above, BBFT shows green fluorescence in the amorphous state but blue in crystals. Thus the conversion to blue emission from the core region indicates the crystallization of this area. To verify the internal morphology in the shell, we used TEM to probe into the particles. As shown in Figure 4e, the TEM image of a particle in this stage reveals a darker color core part than the outer region, indicating a greater density there, resulting from crystallization. More importantly, selected-area electron diffraction of the center of the particle shows obvious diffraction spots (Figure 4f), which provides direct evidence for the occurrence of crystallization inside the microparticle. However the shell of the particle seems quite solid and resistant. Even after extension of the exposure time to 100 h, the outer shell of the particles still shows bright green fluorescence (Figure 4d), suggesting that it remains amorphous. This implies that spontaneous crystal growth from the core cannot penetrate the particle shell to induce the entire particle to crystalize. Because the four fluorescence pictures were taken at the same location, we noticed some changes in Figure 4d compared to the earlier stage, that is, the number of the microparticles decreases and the size of the individual particles increases. This is Ostwald ripening, where small particles dissolve and the dissolved species redeposit on the surfaces of larger particles to provide smaller curvatures and lower energy.

Complete crystallization for a whole particle was found occasionally on some imperfect spheres located at the edges of the substrate (Supporting Information, Figure S2), which indicated us that the solid outside shells are capable of converting when they containing defects. Thus next we manually broke some microparticles with a needle into fragments, and then moved the pieces to contact with the surface of other microparticles. Based on the extent of contact between the particle and the fragment, we categorized the crystallization evolution of these defective microspheres into three cases. As shown in Figure 5, in the first case a fragment

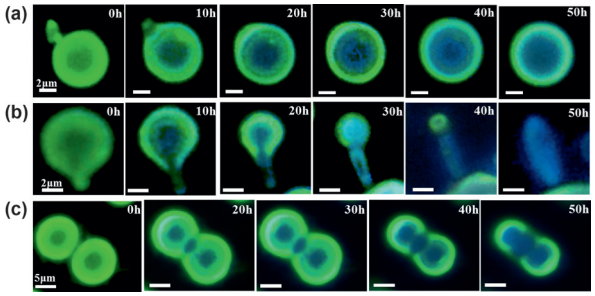

Figure 5. Fluorescence images of the crystallization process due to contact between microparticles. a) Slight contact with a fragment, b) in-depth contact with fragment, and c) twin microparticles. The scale bars in (a) and (b) are 2 μm, and those in (c) are 5 μm.

slightly touched a microsphere surface. The fragment was gradually absorbed by the large particle and became part of it. After 20 h, the fragment had almost totally merged into the microsphere; and in the center of the microsphere had started to crystallize. Later, it behaved like a regular microspheres as described above, the crystallization of which was confined to the inner part of the particle even after 50 h. The situation would be quite different when we moved a fragment heavily and made it strike a microparticle (Figure 5b). In this case crystallization initiated at the contact location as well as at the center of the microsphere. Like a bud sprouts from a seed, the small fragment first grew into a ribbon from the contact surface; then the crystallization from the contact surface and the particle center joined together, making the ribbon longer while the particle became smaller. After 40 h the particle shrank to a little spot with green fluorescence and most of its molecules crystallized on the blue ribbon. The complete crystallization of the round particle resulted in a long rod within 50 h. Another landmark phenomena observed during the crystallization process appeared when two microparticles were close to each other (Figure 5c). The crystallization evolution of the twin microparticles has some similarity with both of the above cases containing fragment contaminant. The centers of the two particles had crystallized prior to contact. Next crystal formed in the contact region; and along with the crystallized parts growing larger, the intermediate

annulus with shallow blue transformed into a deep blue crystalline state. Accompanying the crystallization of the inner parts, the amorphous shells fused together resulting in a uniform shell. The twin microparticles did not completely crystalize, and ended as capsule-like ellipsoids with blue cores encapsulated in green shells that are also present in Figure 4 d.

These three cases plus the regular microspheres reflect the possible crystallization processes of molecular microparticles. From these pictures we can see that in most of the possibilities the external appearance of the microparticles does not change much during the crystallization process; only through fluorescence can we penetrate into the inner structure of the particles to monitor and record the details of the morphology transition during crystallization. In our experiments we also attempted to obtain the three-dimensional images utilizing confocal microscopy. However, perhaps due to the higher density of the solid spheres than that of the cells, and the difference between the monochromaticity of the excitation light (405 nm) in the confocal laser scanning microscopy comparing with the wide distribution (340–380 nm) in the fluorescence microscopy, the tomography image cannot distinguish the two phases.

The evolution of crystallization of the BBFT microparticles was verified by using X-ray diffraction (XRD) patterns, as shown in Figure 6. The as-deposited films of the

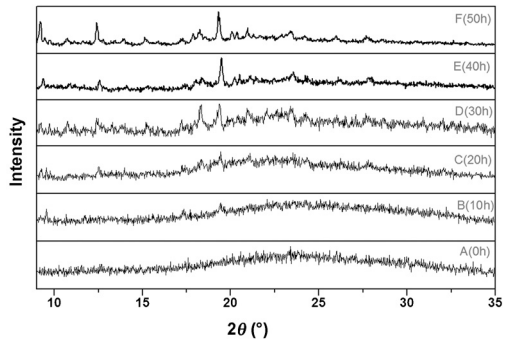

Figure 6. XRD spectra before and after exposure to ethanol vapor for 10, 20, 30, 40, and 50 h.

microparticles did not show any noticeable peaks in the XRD diffraction profile, indicating their amorphous nature. After exposure to ethanol vapor, weak diffraction peaks showed up after 10 h, corresponding to the initial formation of the crystalline cores. On further exposure, the crystallinity increased, and diffraction peaks appeared. After 30 h there were clear reflection peaks, and after 40 h the diffraction patterns showed a high signal-to-noise ratio, indicating a great portion of the microparticles had transformed into the crystallized.

Based on the observed phenomena using fluorescence microscopy, we propose a mechanism model for the ACT of a microparticle. From the observations reported above, it is evident that the molecules in the core of a particle can crystallize more readily than the molecules at the outer surface, even though there is greater stimulus for crystallization at the outer surface where the molecules are in directly in contact with the solvent vapor (the crystallizing stimulus). The solvent vapor acts to provide mobility to the molecules to promote crystallization.[14] The nucleation starts from the center of the microparticle; then the molecules around the nuclei join them to increase the size of the crystalline region. However, the crystal growth from the core does not penetrate the shell, resulting in a core–shell structure, as illustrated in the top part of Figure 7. Of note, this is counter to the Gibbs–

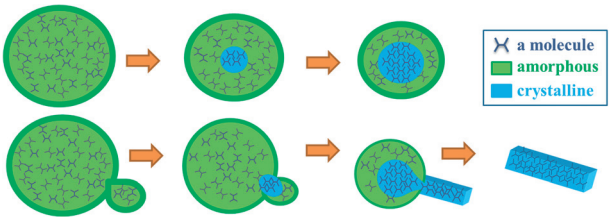

Figure 7. Models of the crystallization process. Top: the crystallization process of a perfect microparticle. Bottom: the crystallization process of a microparticle with a defect.

Thompson theory, based on which the nucleation can be divided into two contributions: a surface (interfacial) term that is energetically unfavorable and a volume term that is energetically favorable. Thus the molecules in the core of a particle were supposed to be less readily to crystallize than those on the exterior surface. Actually a similar phenomenon has been mentioned by Chandaluri et al. in the microparticles of 7,7-diamino-8,8-dicyanoquinodimethanes (DADQs).[11i] Although they did not record the crystallization process by optical or electron microscopy, the SEM images after crystallization revealed nanocrystals inside amorphous shells, which they interpreted to be caused by the hydrophobic interactions of the particle surface with the polymer host materials. In the present case, the host polymer is absent, indicating that the origin of the crystallization from the core of a particle should be an intrinsic behavior of such molecular materials. We have observed that the amorphous outer layer of the microparticle is sufficiently stable so that it resists the growth of the crystal that has nucleated in its interior. The crystallization potential is not strong enough to overcome the barrier presented by the energy level of a perfect spherical shell. The reasons for the stability of this outer amorphous layer are not clear.[15] However, the microparticles are observed to undergo Ostwald ripening, so the stable amorphous surface layer is able to accommodate changes in the size of the microparticle. And when two microparticles come together they can form a twinned microparticle with a stable outer layer, as illustrated in Figure 5.

However, if the shell is broken, the disruption of the perfect spherical shell will lower the barrier to crystallization. Then the growth from the defect conjugates with the crystallization from the core, finally generating a complete crystal, as illustrated in the bottom part of Figure 7. In this situation, the shape of the particle before and after crystallization changes a lot, from a spherical particle to a ribbon-like crystal.

In conclusion, based on a novel organic chromophore with morphology-dependent fluorescence and judicious design of the observation procedure, we have demonstrated the in situ and direct observation of the crystallization process of molecular microparticles. The details of an important solid-state process, the amorphous-to-crystalline transformation, were determined by fluorescence microscopy. The crystallization of an amorphous microparticle was shown to nucleate at its center. However, the growth was confined to the inner part of perfectly spherical microparticles, ending with a core–shell structure. Defects of the surface prior to crystallization can lead to a complete conversion from an amorphous sphere to a ribbon-like crystal. Profiting from the response of the self-fluorescence, the appearance and the interface evolution of the forming crystalline phase inside the particle can be clearly observed. The study presents a realistic picture of the microscopic kinetics of a solid-solid transition, which we believe will deepen the understanding of many solid-state crystallization processes that occur spontaneously in atmosphere or under external stimuli. Furthermore, this facile method may open viable opportunities and inspirations for other observational purposes employing fluorescence microscopy and fluorescent materials, especially for those transitions that lie hidden below the surface.

Keywords: amorphous materials · crystallization · fluorescence microscopy · microparticles · phase transitions

How to cite: *Angew. Chem. Int. Ed.* **2015**, *54*, 7976–7980
Angew. Chem. **2015**, *127*, 8087–8091

[1] a) *Nature* **1870**, *2*, 130; b) C. H. Desch, *Nature* **1926**, *117*, 694–695; c) E. Rideal, *Nature* **1949**, *164*, 303–305.

[2] a) C.-Y. Wu, J. Martel, D. Young, J. D. Young, *PLoS One* **2009**, *4*, e8058; b) H.-H. Peng, J. Martel, Y.-H. Lee, D. M. Ojcius, J. D. Young, *Nanomedicine* **2011**, *6*, 643–658; c) X. Wang, Q. Xu, M. Li, S. Shen, X. Wang, Y. Wang, Z. Feng, J. Shi, H. Han, C. Li, *Angew. Chem. Int. Ed.* **2012**, *51*, 13089–13092; *Angew. Chem.* **2012**, *124*, 13266–13269; d) S. Strydom, W. Liebenberg, L. Yu, M. de Villiers, *Int. J. Pharm.* **2009**, *379*, 72–81; e) D. Xia, J. X. Wu, F. Cui, H. Qu, T. Rades, J. Rantanen, M. Yang, *Eur. J. Pharm. Sci.* **2012**, *46*, 446–454.

[3] a) G. Bollag, P. Hirth, J. Tsai, J. Zhang, P. N. Ibrahim, H. Cho, W. Spevak, C. Zhang, Y. Zhang, G. Habets, *Nature* **2010**, *467*, 596–599; b) A. D. Kwong, R. S. Kauffman, P. Hurter, P. Mueller, *Nat. Biotechnol.* **2011**, *29*, 993–1003.

[4] J. A. Baird, B. Van Eerdenbrugh, L. S. Taylor, *J. Pharm. Sci.* **2010**, *99*, 3787–3806.

[5] N. S. Trasi, J. A. Baird, U. S. Kestur, L. S. Taylor, *J. Phys. Chem. B* **2014**, *118*, 9974–9982.

[6] a) C. Bunn, *Nature* **1964**, *202*, 939–940; b) B. K. McMillin, P. Biswas, M. R. Zachariah, *J. Mater. Res.* **1996**, *11*, 1552–1561; c) J. Ihli, W. C. Wong, E. H. Noel, Y.-Y. Kim, A. N. Kulak, H. K. Christenson, M. J. Duer, F. C. Meldrum, *Nat. Commun.* **2014**, *5*, 3169.

[7] a) F. Zhou, R. Lück, K. Lu, E. Lavernia, M. Rühle, *Philos. Mag. A* **2002**, *82*, 1003–1015; b) D. J. Erskine, W. J. Nellis, *Nature* **1991**, *349*, 317–319; c) R. Z. Khaliullin, H. Eshet, T. D. Kuhne, J. Behler, M. Parrinello, *Nat. Mater.* **2011**, *10*, 693–697; d) P. Burnley, H. Green, *Nature* **1989**, *338*, 753–756; e) K. Jacobs, D. Zaziski, E. C. Scher, A. B. Herhold, A. P. Alivisatos, *Science* **2001**, *293*, 1803–1806.

[8] a) P. Y. Huang, S. Kurasch, J. S. Alden, A. Shekhawat, A. A. Alemi, P. L. McEuen, J. P. Sethna, U. Kaiser, D. A. Muller, *Science* **2013**, *342*, 224–227; b) Z. Tang, Z. Zhang, Y. Wang, S. C. Glotzer, N. A. Kotov, *Science* **2006**, *314*, 274–278; c) D. Li, M. H. Nielsen, J. R. Lee, C. Frandsen, J. F. Banfield, J. J. De Yoreo, *Science* **2012**, *336*, 1014–1018; d) H.-G. Liao, L. Cui, S. Whitelam, H. Zheng, *Science* **2012**, *336*, 1011–1014; e) K. Harano, T. Homma, Y. Niimi, M. Koshino, K. Suenaga, L. Leibler, E. Nakamura, *Nat. Mater.* **2012**, *11*, 877–881; f) M. Sleutel, J. Lutsko, A. E. Van Driessche, M. A. Durán-Olivencia, D. Maes, *Nat. Commun.* **2014**, *5*, 5598.

[9] a) T. H. Zhang, X. Y. Liu, *Angew. Chem. Int. Ed.* **2009**, *48*, 1308–1312; *Angew. Chem.* **2009**, *121*, 1334–1338; b) U. Gasser, E. R. Weeks, A. Schofield, P. Pusey, D. Weitz, *Science* **2001**, *292*, 258–262; c) P. Tan, N. Xu, L. Xu, *Nat. Phys.* **2014**, *10*, 73–79.

[10] R. Y. Tsien, *Annu. Rev. Biochem.* **1998**, *67*, 509–544.

[11] a) Z. Chi, X. Zhang, B. Xu, X. Zhou, C. Ma, Y. Zhang, S. Liu, J. Xu, *Chem. Soc. Rev.* **2012**, *41*, 3878–3896; b) Y. Dong, J. W. Lam, A. Qin, Z. Li, J. Sun, H. H.-Y. Sung, I. D. Williams, B. Z. Tang, *Chem. Commun.* **2007**, 40–42; c) L. Qian, B. Tong, J. Shen, J. Shi, J. Zhi, Y. Dong, F. Yang, Y. Dong, J. W. Lam, Y. Liu, *J. Phys. Chem. B* **2009**, *113*, 9098–9103; d) X. Zhang, Z. Chi, Y. Zhang, S. Liu, J. Xu, *J. Mater. Chem. C* **2013**, *1*, 3376–3390; e) H. Ito, M. Muromoto, S. Kurenuma, S. Ishizaka, N. Kitamura, H. Sato, T. Seki, *Nat. Commun.* **2013**, *4*, 2009; f) T. Seki, K. Sakurada, H. Ito, *Angew. Chem.* **2013**, *125*, 13062–13066; g) Y. Zhang, K. Wang, G. Zhuang, Z. Xie, C. Zhang, F. Cao, G. Pan, H. Chen, B. Zou, Y. Ma, *Chem. Eur. J.* **2014**, *21*, 2474—2479; h) J. Wang, J. Mei, R. Hu, J. Z. Sun, A. Qin, B. Z. Tang, *J. Am. Chem. Soc.* **2012**, *134*, 9956–9966; i) C. G. Chandaluri, T. Radhakrishnan, *Angew. Chem. Int. Ed.* **2012**, *51*, 11849–11852; *Angew. Chem.* **2012**, *124*, 12019–12022.

[12] Y. Lv, Y. Liu, D. Guo, X. Ye, G. Liu, X. Tao, *Chem. Asian J.* **2014**, *9*, 2885–2890.

[13] Y. Lv, Y. Liu, X. Ye, G. Liu, X. Tao, *CrystEngComm* **2015**, *17*, 526–531.

[14] a) S. H. Kim, M. J. Misner, T. Xu, M. Kimura, T. P. Russell, *Adv. Mater.* **2004**, *16*, 226–231; b) K. W. Gotrik, C. Ross, *Nano Lett.* **2013**, *13*, 5117–5122.

[15] a) A. I. Toldy, L. Zheng, A. Z. M. Badruddoza, T. A. Hatton, S. A. Khan, *Cryst. Growth Des.* **2014**, *14*, 3485–3492; b) D. Horn, J. Rieger, *Angew. Chem. Int. Ed.* **2001**, *40*, 4330–4361; *Angew. Chem.* **2001**, *113*, 4460–4492; c) P. R. ten Wolde, D. Frenkel, *Phys. Chem. Chem. Phys.* **1999**, *1*, 2191–2196.

Received: April 2, 2015
Published online: May 14, 2015

